Structural characterization of Ti-15Mo alloy used as biomaterial by Rietveld method

José Roberto Severino Martins and Carlos Roberto Grandini

Additional information on J. Appl. Phys.

Structural characterization of Ti-15Mo alloy used as biomaterial by Rietveld method

José Roberto Severino Martins Jr. and Carlos Roberto Grandini[a]
UNESP - Univ. Estadual Paulista, Laboratório de Anelasticidade e Biomateriais, 17.033-360, Bauru, SP, Brazil

The biochemical and mechanical behavior of titanium alloys has been studied extensively for a variety of applications in the aerospace and biomedical fields. In the literature, there are studies that relate the microstructure and the phases of the material with its properties; however, there is little information that quantifies each phase and relates this to its properties. In addition, little has been done to analyze the effects of oxygen and heat treatment on the alloy's structure. In this paper, the effect of doping with oxygen and the effect of heat treatments on structural properties of Ti-15Mo alloy used as biomaterials is examined using scanning electron microscopy, x-ray diffraction, and diffractogram analysis using the Rietveld method. © *2012 American Institute of Physics*. [http://dx.doi.org/10.1063/1.4707920]

I. INTRODUCTION

The developing area of biomaterials involves finding materials with physical properties that are both minimally toxic and compatible with human tissue. Materials that exhibit this great combination are titanium and its alloys. In this way, titanium and several of its alloys have been widely used in the manufacture of prostheses and special devices in the medical and dental care areas, since 1970, due to its properties of low elasticity modulus values (Young modulus), corrosion resistance, and biocompatibility.[1–3]

Ti-6Al-4 V is the titanium alloy that is most frequently used for biological applications, and its stoichiometry varies slightly, depending on the default chosen by the manufacturer. The higher the content of oxygen, nitrogen, or vanadium, the greater is their strength. The inverse is true as well; the lower the content of these elements, the greater is the fracture toughness, ductility, and corrosion resistance. However, recently it was discovered that vanadium causes cytotoxic effects and adverse reactions in some tissues,[4] while aluminum has been associated with neurological disorders.[5,6] In addition, the elasticity modulus of this alloy is around 120 GPa, which is well above that of the human bone (around 28 GPa). Thus, many surveys have sought alternatives to Ti-6Al-4 V alloy in an attempt to obtain alloys with similar (or higher) mechanical strength, lower elasticity modulus, and improved biocompatibility. The most promising are those alloys that present niobium, zirconium, molybdenum, and tantalum as alloying elements added to titanium.[2] Recently, alloy containing β phase stabilizers elements (niobium, tantalum, zirconium, and molybdenum) with lower values of Young's modulus have been considered attractive for employment as biomaterials, among which the Ti-Mo alloy systems stand out.[7–13]

The Ti-Mo alloy systems were studied with an emphasis on their microstructure and mechanical properties, specifically on phase transformations,[10] mechanical resistance,[14] and corrosion.[15] However, there are few studies on the processing of these alloys with specific properties, the influence of thermo-mechanical treatments, and about the effect of interstitial elements on their mechanical properties.[13]

Among the alloys of the Ti-Mo system, the Ti-15Mo alloy possesses excellent corrosion resistance and a good combination of mechanical properties such as fatigue, hardness, and wears resistance. This alloy demonstrates good properties for biomedical applications and is already included in the American Society for Testing and Materials;[16] however, the effects of oxygen and heat treatments on its structure and microstructure have not yet been analyzed.

The main objective of this paper is the structural and microstructural characterization of the Ti-15Mo alloy after heat treatments and oxygen doping using the Rietveld method as a tool.

II. EXPERIMENTAL DETAILS

The samples used in this paper are titanium alloys containing 15% (in weight) of molybdenum. Such samples were produced in the Laboratório de Anelasticidade e Biomateriais (UNESP/Bauru) using an arc-melting furnace (for further details of preparation see Ref. 17). Titanium cp (99.7% of purity) and molybdenum (99.5% of purity) were used; both were acquired from Aldrich Inc. The materials were remelted at least five times to ensure homogeneity. After melting, an ingot was obtained, which was later passed through a hot swaging machine in the Laboratório de Fusão por Feixe de Elétrons e Tratamentos Termomecânicos of Unicamp, where it was obtained cylindrical bars with 4.0 mm diameter by 60.0 mm length. Then, homogenization heat treatment was conducted, which consisted of heating the sample at a rate of 10 K/min up to the level of 1273 K over 24 h and then cooled slowly after this period. The sample was named Ti-15Mo#0 (after melting), Ti-15Mo#1 (after hot swaging), and Ti-15Mo#3 (after heat treatment). After heat treatment, the samples were doped with oxygen, heating the samples at a 10 K/min rate up to a plateau

---

a)Author to whom correspondence should be addressed. Electronic mail: betog@fc.unesp.br. Tel./Fax: +55-14-31036179.

TABLE I. Chemical composition of the Ti-15Mo#0 sample.[17]

Element	Mo	Cr	Fe	Ni	Ti
wt. %	14.47	0.008	0.024	0.007	Balance

TABLE II. Oxygen and nitrogen concentrations in the Ti-15Mo samples used in this paper.

Sample	Oxygen (wt. %)	Nitrogen (wt. %)
Ti-15Mo#0	0.137 ± 0.005	0.006 ± 0.001
Ti-15Mo#1	0.177 ± 0.004	0.007 ± 0.002
Ti-15Mo#2	0.223 ± 0.002	0.009 ± 0.002
Ti-15Mo#3	0.251 ± 0.008	0.020 ± 0.002
Ti-15Mo#4	0.229 ± 0.005	0.018 ± 0.003
Ti-15Mo#5	0.204 ± 0.008	0.015 ± 0.003

of 700 K, and then oxygen was introduced with partial pressures of 5×10^{-1} Torr (sample Ti-15Mo#3), 1.6×10^{-2} Torr (sample Ti-15Mo#4), and 1.6 Torr (sample Ti-15Mo#5). Samples Ti-15Mo#3 and #4 were in the plateau for 2 h, while sample Ti-15Mo#5 was in the plateau for 3 h. After that the samples were quickly cooled with water until they reached ambient temperature.

The chemical composition analysis to determine the elements of interest was made using an optical induced plasma emission spectrometer, model Vista, Varian Inc. Table I shows the obtained results.

For the gas analysis, the method used was melting the samples under inert gas with infrared detection for oxygen and thermal conductivity differences for nitrogen. A LECO TC-400 gas analyzer was used. Table II shows the obtained results.

The x-ray diffraction measurements were carried out using a Rigaku D/Max 2100/PC equipment with radiation Cu-Kα of $\lambda = 1.544$ Å, a fixed time mode with a step of 0.02, a permanence time of 1.6 s, and a scan of 10 to 100°.

The SEM measurements were performed in a FEI equipment model Quanta 400. The energy dispersive spectroscopy (EDS) mapping was obtained in an Oxford equipment model INCA Energy 250.

III. RESULTS AND DISCUSSION

The results of the chemical composition of the Ti-15Mo#0 sample, presented in Table I, show that the molybdenum concentration is 14.47 wt. %, which is accordance with the ASTM F 2066-08[16] that establishes a tolerance of 14 to 16 wt. % of molybdenum.

Fig. 1 shows EDS mapping of the elements that compose the alloy. In Fig. 1(a), the molybdenum element's distribution in the Ti-15Mo alloy is represented by the light regions. In Fig. 1(b), the titanium element's distribution in the Ti-15Mo alloy is represented by the dark regions. Figure 1(c) shows the overlap of Figures 1(a) and 1(b), illustrating the homogeneous distribution (homogeneous distribution of light and dark points) of alloying elements at a 500x magnification. Figure 1 thus demonstrates a homogenous distribution of alloying elements rather than the formation of segregated regions, i.e., regions with the largest concentrations of a given element.

The analysis of gas content presented in Table II shows that the Ti-15Mo#0 sample has oxygen and nitrogen dissolved interstitially in small quantities from the melting process. With the hot swaging (Ti-15Mo#1) sample, oxygen and nitrogen were incorporated, which was expected since the heat was set at room temperature, enabling the incorporation of interstitial elements. Following the heat treatment (Ti-15Mo#2 sample), the increase of interstitials is explained
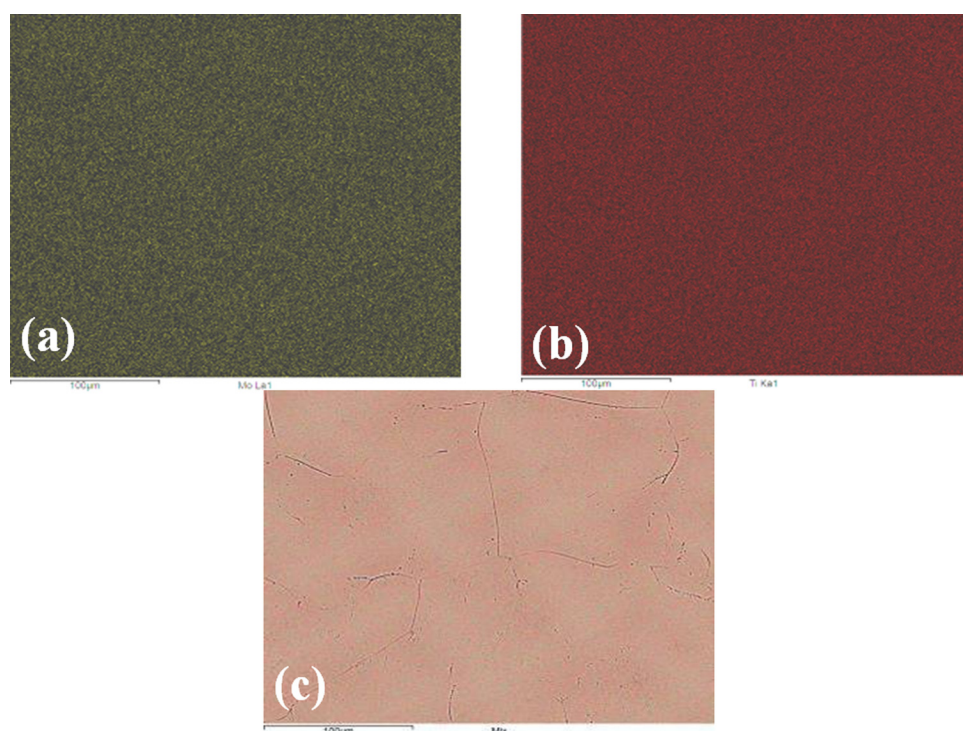

FIG. 1. EDS mapping for the Ti-15Mo#0 sample. (a) Molybdenum mapping; (b) titanium mapping; and (c) titanium and molybdenum mapping.

by the possible presence of impurities on the surface of the quartz tube; when heated, they are released to the inside of the tube and the sample ends up absorbing them. With the first doping with oxygen (Ti-15Mo#3 sample), there was a significant increase in the oxygen concentration, which was expected. However, the amount of nitrogen doubled in relation to the thermally treated sample, which can also be explained by the tube's contamination, with these impurities being incorporated in the sample. After the second (Ti-15Mo#4 sample) and third (Ti-15Mo#5 sample) doping, there was a decrease in the oxygen and nitrogen content in relation to the first doping. This decrease in the concentration of interstitial elements can be explained by the fact that the first two doping processes successively diffused less oxygen inside of the samples due to the presence of oxides on the surface hindering the diffusion of oxygen into the samples. By ASTM F 2066-08 (Ref. 16), the maximum levels (in wt. %) tolerated for oxygen and nitrogen are 0.20 ± 0.02 and 0.05 ± 0.02, respectively. Table II illustrates that the content of oxygen and nitrogen in the Ti-15Mo#0 and Ti-15Mo#1 samples is in accordance with the established standard, which shows that the sample was prepared properly. In the case of Ti-15Mo#2, Ti-15Mo#3, and Ti-15Mo#4 samples, the content of nitrogen is within the standard, but the oxygen content is above. However, this is not problematic because the purpose of this paper is to study oxygen's effect on the properties of this alloy. For the Ti-15Mo#5 sample, there was a decrease in oxygen and nitrogen levels, which is consistent with the standard.

The results of the x-ray diffraction measurements for Ti-15Mo and cp-Ti samples studied in this paper are shown in Figure 2. The structural modification occurs with the addition of 15 wt. % molybdenum to titanium and changes from the hexagonal structure to a structure with β phase predominance. These results clearly show that the crystalline structure of the Ti-Mo system is sensitive to the molybdenum composition, as mentioned in the literature.[18] It can also 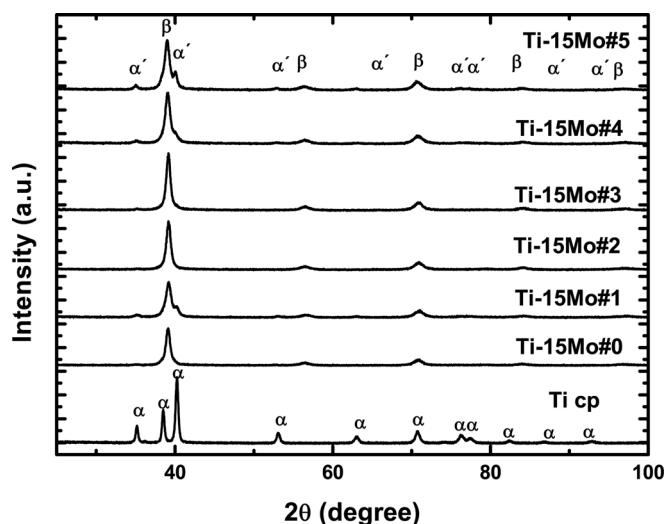be observed that the diffractograms of the Ti-15Mo alloy showed peaks characteristic of a body-centered cubic structure, which is typical of these phase β alloys[8,12] and α' phase that has hexagonal compact crystalline structure, but this last phase is a martensitic type phase, i.e., it is a metastable phase that is formed by rapid cooling, leaving no time to accommodate a more stable structure.

From the x-ray diffractograms, a series of information can be obtained. The position of the peaks provides information about the unit cell dimensions, the crystalline system, and the identification of crystalline phases. The intensity of the peaks provides the unit cell contents and enables qualitative analysis of the phases, while the shape and width of the peaks are related to the size of lattice defects and crystallites.[19]

From the peak's position, it is possible to see that there are two crystalline phases, the β phase and the α' phase. These phases are present in every condition of Ti-15Mo alloy processing. In the Ti-15Mo#0 sample, the peaks of the α' phase are less intense, which indicates that this phase is present in a very small amount. According to Bania et al.,[18] at room temperature, above 10% in weight of molybdenum, β phase is predominant. However, in the sample Ti-15Mo#1 it can be seen by the diffractogram (Fig. 2) that there was an increase of α' phase intensity, which is explained by the fact that the sample was heated and suffered a cooling that eventually led to the formation of the α' phase. In the sample Ti-15Mo#2, which suffered a homogenization heat treatment, there was a decrease of the peaks that appeared after the swaging, showing that there was a phase recovery. This was expected since the temperature was above the transformation temperature and cooling was slow, so part of the α' phase was transformed to a β phase. After oxygen doping, there was always an increased peak intensity in the α' phase, being that in the third doping (Ti-15Mo #5 sample), there was a large increase; thus, it is possible to observe the peak's superposition. This is because doping requires fast cooling with water, which leads to the formation of a non-equilibrium structure, the α' phase. As doping was successively performed in the samples, the α' phase incrementally increased; the presence of α' phase peaks is illustrated in the time-temperature-transformation (TTT) diagram of the Ti-15Mo alloy.[20] As the peak intensities varied after processing, this can be associated with the concentration of phases[21,22] because the microstructure of the samples varied after processing. In order to evaluate this effect, x-ray diffractograms were refined using the Rietveld method.[21]

For the analysis of x-ray diffractograms, the General System Analyzer Structure (GSAS) software[23] and the PV-TCHZ (pseudo-Voigt Thompson-Cox-Hastings) profile adjustment function were used. The crystallographic sheets used to obtain crystallographic information for the β phase was the record no. 644489-ICSD (Inorganic Crystal Structure Database) and the record no. 653280-ICSD was used for the α' phase, both from the ICSD.[24]

Figs. 3–8 show the diffractograms analyzed using the Rietveld method, where great concordance of measured and calculated data can be observed, showing that refinement was done fairly satisfactory. The merit indexes are showed in Table III and are consistent with the literature,[25] which

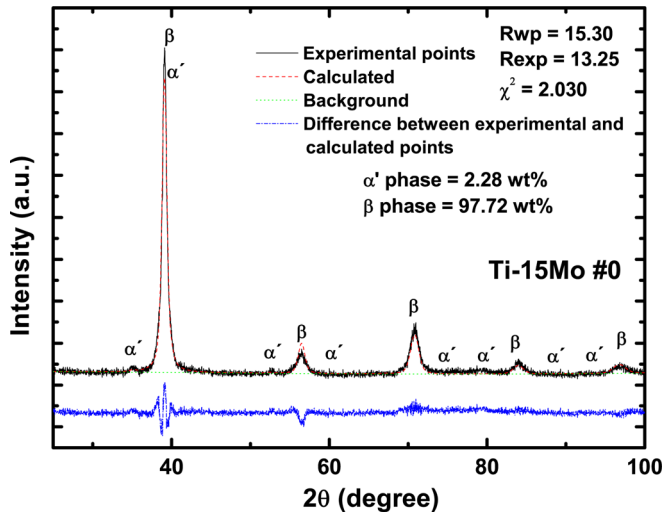FIG. 2. X-ray diffractograms for the Ti-15Mo alloy samples used in this paper, compared with cp-Ti.

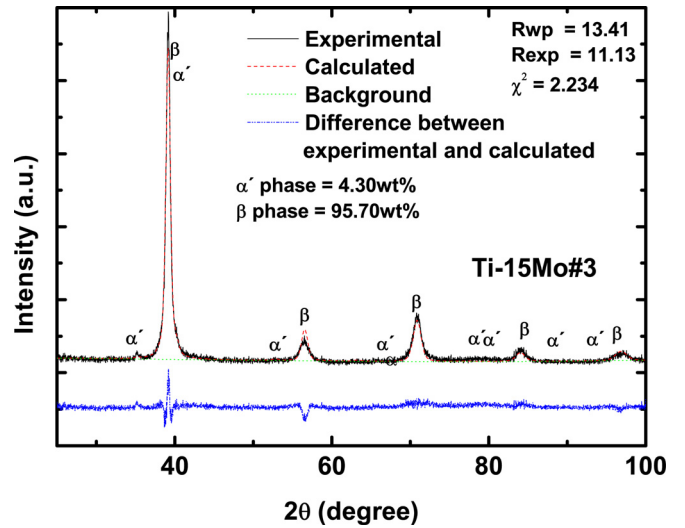FIG. 3. X-ray diffractogram analyzed using the Rietveld method for the Ti-15Mo#0 sample.

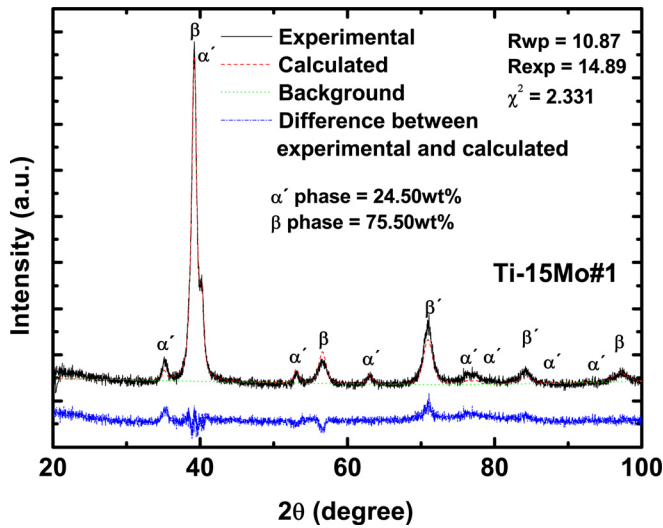FIG. 6. X-ray diffractogram analyzed using the Rietveld method for the Ti-15Mo#3 sample.

FIG. 4. X-ray diffractogram analyzed using the Rietveld method for the Ti-15Mo#1 sample.
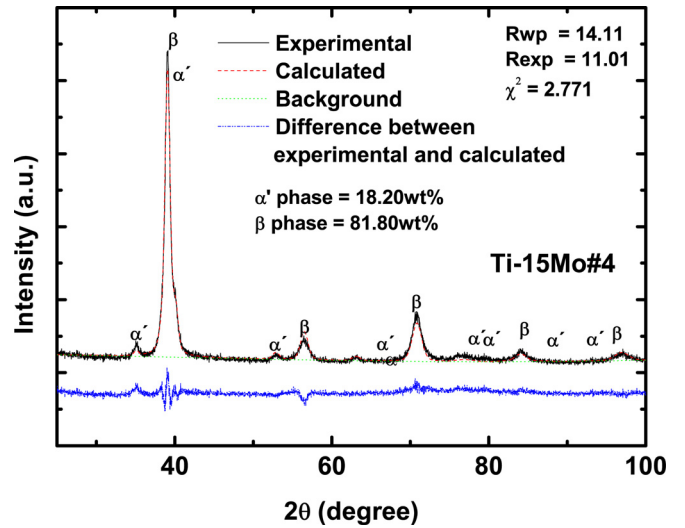

FIG. 7. X-ray diffractogram analyzed using the Rietveld method for the Ti-15Mo#4 sample.
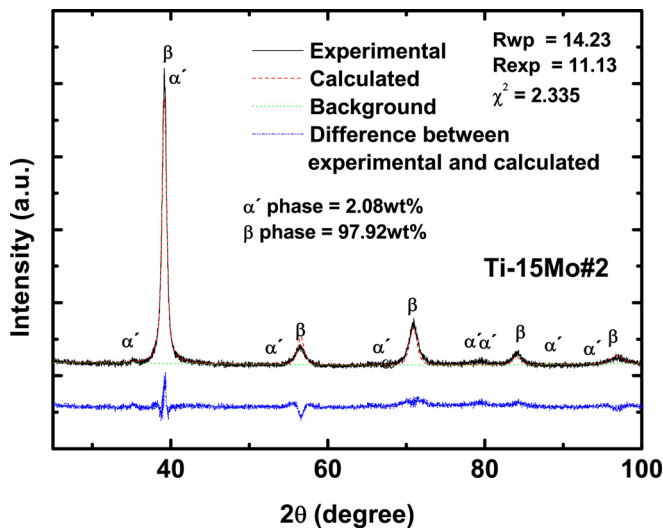

FIG. 5. X-ray diffractogram analyzed using the Rietveld method for the Ti-15Mo#2 sample.
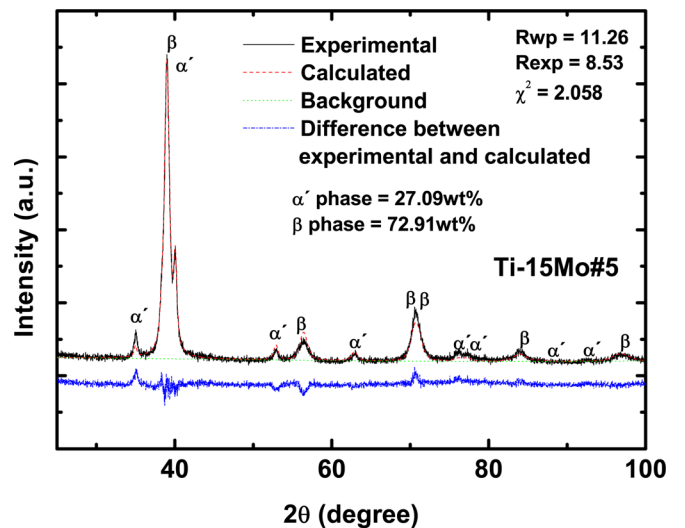

FIG. 8. X-ray diffractogram analyzed using the Rietveld method for the Ti-15Mo#5 sample.

TABLE III. Statistical parameters of the Rietveld refinement.

Sample	R_{exp}	R_{wp}	χ^2
Ti-15Mo#0	13.25	15.43	2.030
Ti-15Mo#1	10.87	14.09	2.331
Ti-15Mo#2	11.13	14.23	2.335
Ti-15Mo#3	10.38	13.41	2.234
Ti-15Mo#4	11.01	14.11	2.771
Ti-15Mo#5	8.53	11.26	2.058

enhances the quality of refinement. The values of the quantities of each phase and the lattice parameters are shown in Table IV. Moreover, after each processing, the Ti-15Mo alloy samples' microstructure suffered variations both in the phase's proportions and in the lattice parameters.

After melting, the Ti-15Mo#0 sample had a microstructure of α'–β with β phase predominance. The swaging (Ti-15Mo#1 sample) provided an increase in the quantity of phase α', due to the fact that the sample was heated for swaging and the cooling retained phase α'. With the homogeneity heat treatment (Ti-15Mo#2 sample), there was β phase recovery, and the sample's proportion increased and returned to its original size, which is explained by the fact that treatment achieved a temperature greater than the β transformation temperature and the cooling was slow, i.e., possessing the time required for the crystalline structure to accommodate a smaller energy configuration, in this case, the β phase. With oxygen doping (Ti-15Mo#3, Ti-15Mo#4, and Ti-15Mo#5 samples), there was a successive increase in the amount of the α' phase, which can be explained by the fact that the sample was heated to 700 °C and underwent rapid cooling, thus retaining the α' phase, in accordance with the TTT diagram for this material.[20]

As for the lattice parameters, these varied after each processing. The sample taken after melting, Ti-15Mo#0, had the highest reason c/a and β phase lattice parameter values. The high value of reason c/a is greater because of the hexagonal structure, which has been distorted because the water cooled the crucible. The temperature gradient that existed in the crucible during the solidification process distorted the hexagonal structure. After swaging (Ti-15Mo#1 sample), there was a decrease in the β phase lattice parameter and also the reason c/a of the α' phase. This can be explained by the function of the large phase α' concentration increase, in addition to internal stresses, which eventually distorted the crystalline lattice, decreasing the lattice parameter of the β phase. After homogeneity heat treatment (sample

Ti-15Mo#2), the β phase lattice parameter recovered, but the value of reason c/a decreased; this is related to the increased phase β, which "compressed" the α' phase. Here, the role of oxygen must also be accounted for, which enters interstitially in the β phase, distorting the crystal structure to increase the lattice parameter. Due to the high packaging factor of the α' phase, oxygen has great difficulty entering the unit cell interstitially without causing distortion. After the first oxygen doping (Ti-15Mo#3 sample), the lattice parameter of the β phase decreased. As the amount of oxygen was higher in this condition, a greater distortion of the lattice was expected to increase the lattice parameter; however, the α' phase increased its reason c/a and "compressed" the β phase, explaining the decline of its lattice parameter. After the second and third doping (Ti-15Mo#4 and Ti-15Mo#5 samples, respectively), the oxygen content decreased and the α' phase increased in relation to the Ti-15Mo#3 sample, in such a way that the β phase lattice parameter of both decreased.

With the objective of gaining a better understanding of the microstructure, measures of scanning electron microscopy were carried out, whose micrographies with magnification of 1000× for samples of Ti-15Mo alloys used in this paper are presented in Figure 9. The Ti-15Mo#0 sample shows small and irregularly shaped grains, similar to a dendrite structure that is characteristic of the β phase, as can be seen in Figure 9(a). Through Rietveld refinement, a concentration of around 2.30 wt. % was obtained for the α' phase, which cannot be seen in the SEM micrograph due to its low concentration. After swaging (Ti-15Mo#1 sample), there was a different conformation: the grain became smaller and more irregularly shaped, which is characteristic of materials that have passed through thermomechanical processes, as can be seen in Figure 9(b). The intragrain region has lamellae due to plastic deformation caused by swaging, and the α' phase is within these lamellae, having about 25 wt% of this phase on microstructure of the Ti-15Mo#1 sample. **After the homogeneity heat treatment (Ti-15Mo#2 sample), it can be seen in Figure 9(c) that there was a large increase in the grain sizes, which is related to the supply of energy to the system that allowed the growth. Using Rietveld refinement, a concentration of around 2.1 wt. % was obtained for the α' phase, which is not visible with the SEM micrograph due to its low concentration, similar to the Ti-15Mo#0 sample. With the first oxygen doping (sample Ti-15Mo#3), it was not possible to observe a new increase in grain, as can be seen in Figure 9(d). However, a martensite structure emerged, which is characteristic of titanium and its alloys that have undergone rapid cooling. Martensitic phases in titanium alloys can

TABLE IV. Values found for the concentrations of the phases and lattice parameters.

Sample	β phase (wt. %)	a = b = c (Å)	α' phase (wt%)	a = b (Å); c (Å)	c/a
Ti-15Mo#0	97.72	3.2637 ± 0.0006	2.28	2.69 ± 0.02; 4.69 ± 0.05	1.74
Ti-15Mo#1	75.50	3.2564 ± 0.0008	24.50	2.953 ± 0.002; 4.690 ± 0.004	1.59
Ti-15Mo#2	97.92	3.2631 ± 0.0005	2.08	2.82 ± 0.01; 4.08 ± 0.02	1.48
Ti-15Mo#3	95.70	3.2624 ± 0.0005	4.30	2.950 ± 0.003; 4.73 ± 0.01	1.60
Ti-15Mo#4	81.80	3.2582 ± 0.0006	18.20	2.948 ± 0.003; 4.703 ± 0.007	1.60
Ti-15Mo#5	72.91	3.2594 ± 0.0007	27.09	2.954 ± 0.002; 4.695 ± 0.003	1.59

(a)   **(b)**   **(c)**
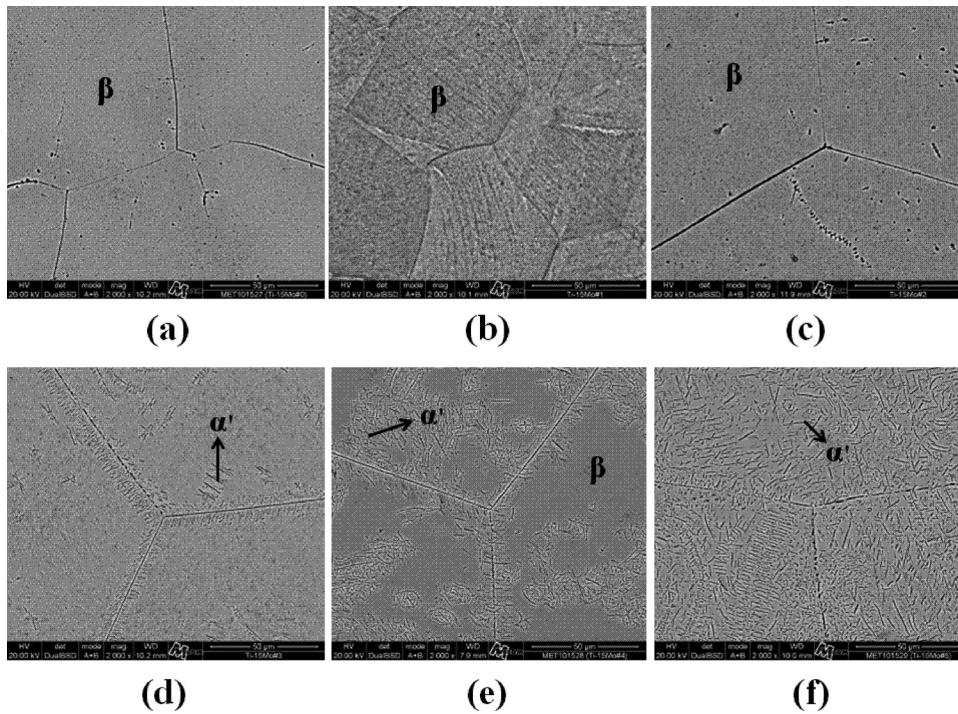

(d)   **(e)**   **(f)**

FIG. 9. Micrographies, with magnification of 1000X, for the: (a) Ti-15Mo#0, (b) Ti-15Mo#1, (c) Ti-15Mo#2, (d) 15Mo#3, (e) Ti-15Mo#4, and (f) Ti-Mo#5 samples.

be of three types: α' (hexagonal), α'' (orthorhombic), and α''' (face centered orthorhombic). From the peak position, it is possible to identify the α' phase, which is hexagonal. Using Rietveld refinement, it was possible to quantify this phase as having 4.30 wt. %. This phase has acicular form and it is distributed in the grain boundaries and spread throughout the sample. After the second doping (Ti-15Mo#4 sample), the martensite phase increased, as can be seen in Figure 9(e). This phase is α' and it is distributed from the grain boundaries and certain regions within the grains. In Figure 9(f), after the third doping (Ti-15Mo#5 sample), it can be observed that the martensite phase α' is distributed homogeneously throughout the grain boundary region and does not have highly concentrated regions.

According to ASTM F 2066-08,[16] the microstructure of the Ti-15Mo alloy can have either a β or α-β structure after annealing. To have a β structure, the Ti-15Mo alloy must be completely recrystallized in the β phase, and the α phase should not be observed at a magnification of 100 times. To have a structure of α-β, the microstructure should be a thin scattering of α and β phases resulting from processing in α-β. The Ti-15Mo# 2 sample would be considered β by ASTM F 2066-08 (Ref. 16) since, even with a magnification of

2000$\times$ in a scanning electron microscope, it was not possible to observe the martensite α' phase. However, the x-ray diffractograms showed the α' phase peaks, and the concentration of this phase was calculated using the Rietveld method, which showed that this sample does not have an exclusively β microstructure. One interesting point is that in the micrographies presented, it was not possible to see the structures of the α' phase, since, by the F 2066-08 standard, the microstructure should be β. However, analyzing the x-ray diffractogram using the Rietveld method permitted the quantification of the α' and β phases, showing that the microstructure of the alloy is α-β. This generates a deadlock, because depending on the technique used to characterize the microstructure, either by electron microscopy or quantitative analysis from x-ray diffraction, errors can occur in the standings since micrographies have limitations when detecting low concentrations of other phases. The x-ray diffraction

TABLE V. Crystallite size and micro-strain of the crystalline lattice for all samples studied.

Sample	% at Mo	D (nm) β	ε (%) β
Ti-15Mo#0	8.09	31 ± 1	0.50 ± 0.01
Ti-15Mo#1	8.09	48 ± 4	0.80 ± 0.01
Ti-15Mo#2	8.09	18 ± 3	0.20 ± 0.06
Ti-15Mo#3	8.09	33 ± 2	0.50 ± 0.05
Ti-15Mo#4	8.09	31 ± 3	0.70 ± 0.01
Ti-15Mo#5	8.09	41 ± 4	0.50 ± 0.03

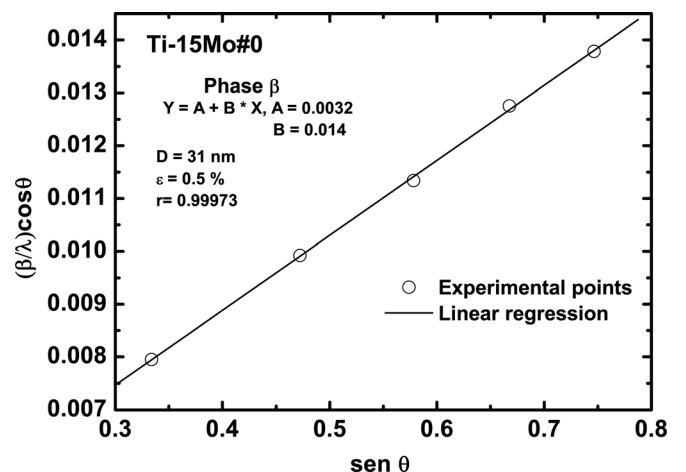FIG. 10. Williamson-Hall graph for the Ti-15Mo#0 sample.

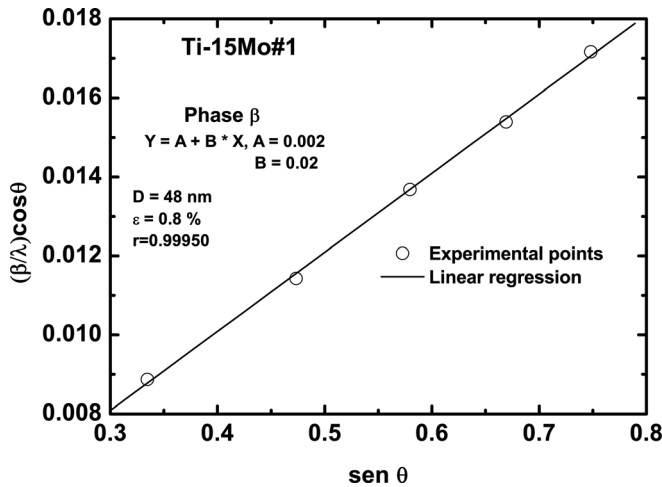FIG. 11. Williamson-Hall graph for the Ti-15Mo#1 sample.

FIG. 13. Williamson-Hall graph for the Ti-15Mo#3 sample.

analysis, if not performed quantitatively, can also induce the errors since it only allows qualitative information to be gathered. Thus, the Rietveld method is the most appropriate since it permits quantitative analysis of the microstructure with reliable results.

Ti-15Mo# 3, #4, and #5 samples were treated in the α-β field and through samples' micrographies it is possible to observe the formation of martensite, classified, therefore as α-β. The ASTM F 2066-08 standard[16] establishes that the α-β microstructure must be a fine dispersion of the α' phase, and the sample that satisfies such condition is the Ti-15Mo#5. The Ti-15Mo#5 sample, therefore, is within the microstructure and the oxygen and nitrogen content specifications.

Williamson-Hall[26] (a method that permits extraction of the structural parameters from linear and angular coefficients of Eq. (1), the crystallite size, and micro-strain) method was used to obtain the average size of the crystallite (see Table V). Once the sample underwent thermo-mechanical treatments, there was a reasonable amount of micro-strain, which is important to take into consideration because it can influence the crystallite's value, and this has not been used the Scherrer[19] equation,

$$\frac{\beta \cdot \cos\theta}{\lambda} = \frac{k}{D} + \frac{4 \cdot \varepsilon \cdot \sin\theta}{\lambda}, \qquad (1)$$
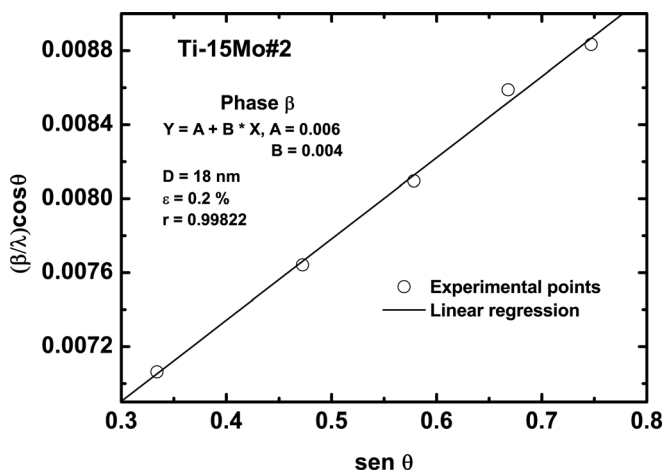
where β is the peak width at half the height of the diffraction peak; λ is the x-ray wavelength; D is the average size of the crystallite; ε is the micro-strain; and k is a constant with value 1.

Figs. 10–15 illustrate the Williamson-Hall of the β phase for all samples used in this paper. All graphics have a correlation coefficient (r) exceeding 0.99, which shows that the linear regression performed was suitable for studying the experimental points based on the Williamson-Hall method that requires great linearity. The size of the crystallite (D) and the micro-strain of the β phase are presented in Table V. For all conditions, the crystallites were small (between 18 and 48 nm), which justifies their broad peaks. An interesting point to note is that the larger sizes of crystallite were in the samples with higher amounts of the α' phase. For micro-strain, after the swaging (Ti-15Mo#1 sample), a large increase was observed in the sample in the after melting condition (Ti-15Mo#0 sample), which was expected since the swaging is too aggressive for the material, generates significant internal stress and distorts the crystalline lattice. Following the homogeneity treatment (Ti-15Mo#2 sample), the micro-strain value decreased by more than 4 times when these internal stresses were relieved. After oxygen doping (Ti-15Mo#3, #4, and #5

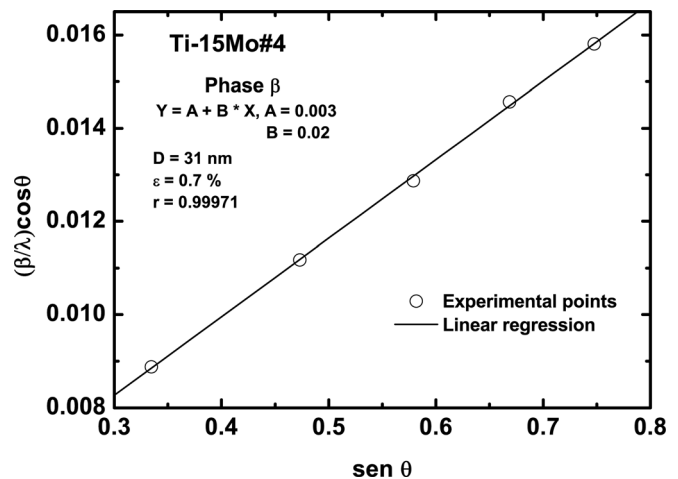FIG. 12. Williamson-Hall graph for the Ti-15Mo#2 sample.

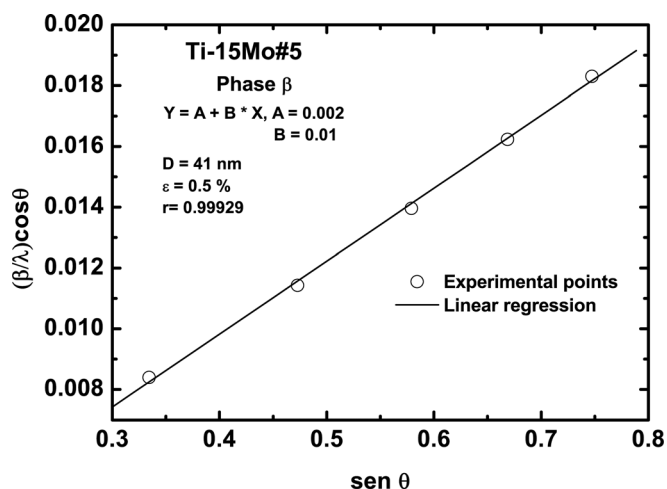FIG. 14. Williamson-Hall graph for the Ti-15Mo#4 sample.

FIG. 15. Williamson-Hall graph for the Ti-15Mo#5 sample.

samples), there was a further increase in micro-strain; this is justified by the increase in the quantity of phase α', which ended up generating more internal stress in the β phase. All values of micro-strain were positive, which means that the crystalline lattice had an expansive stress.

IV. CONCLUSIONS

With this paper, it was possible to characterize the structure and microstructure of the Ti-15Mo alloy, as well as to identify the crystalline phases and to quantify their proportions using the Rietveld method.

By analyzing the x-ray diffractograms using the Rietveld method after melting, swaging, homogenization heat treatment, and oxygen doping, changes were observed in the structural parameters. The micrographies performed corroborate with x-ray diffraction measurements that indicate β phase with a bcc structure and α' phase with an hcp structure, respectively. The results show that the oxygen quantity does not influence the amount of α' phase, while heat treatments with successive cooling increases this phase, as in the samples Ti-15Mo#3, Ti-15Mo#4, and Ti-15Mo#5.

In addition, the use of the Williamson-Hall method permitted the analysis of the influences of processing on the crystallite size and microdeformation of the β phase; along with this, it has been possible to relate changes in form and in the intensity of the x-ray diffractogram peaks after processing.

[1]K. Wang, Mater. Sci. Eng., A **213**(1-2), 134–137 (1996).
[2]M. Geetha, A. K. Singh, R. Asokamani, and A. K. Gogia, Prog. Mater. Sci. **54**(3), 397–425 (2009).
[3]M. Long and H. J. Rack, Biomaterials **19**(18), 1621–1639 (1998).
[4]S. G. Steinemann, in *Evaluation of Biomaterials*, edited by G. D. Winter, J. L. Leray, and K. d. Groot (John Wiley, New York, 1980).
[5]D. R. C. McLachlan, B. Farnell, and H. Galin, in *Biological Aspects of Metals and Metalrelated Disease*, edited by B. Sarkar (Ravon, New York, 1983).
[6]D. P. Perl and A. R. Brody, Science **208**(4441), 297–299 (1980).
[7]M. Sugano, Y. Tsuchida, T. Satake, and M. Ikeda, Mater. Sci. Eng., A **243**(1-2), 163–168 (1998).
[8]W. F. Ho, C. P. Ju, and J. H. Chern Lin, Biomaterials **20**(22), 2115–2122 (1999).
[9]W.-F. Ho, J. Alloys Compd. **464**(1-2), 580–583 (2008).
[10]E. Sukedai, D. Yoshimitsu, H. Matsumoto, H. Hashimoto, and M. Kiritani, Mater. Sci. Eng., A **350**(1-2), 133–138 (2003).
[11]H. Guo and M. Enomoto, Scr. Mater. **54**(7), 1409–1413 (2006).
[12]N. T. C. Oliveira, G. Aleixo, R. Caram, and A. C. Guastaldi, Mater. Sci. Eng., A **452-453**, 727–731 (2007).
[13]R. A. Nogueira, C. R. Grandini, and A. P. R. A. Claro, J. Mater. Sci. **43**(17), 5977–5981 (2008).
[14]M. Niinomi, Mater. Sci. Eng., A **243**(1-2), 231–236 (1998).
[15]N. T. C. Oliveira and A. C. Guastaldi, Corros. Sci. **50**(4), 938–945 (2008).
[16]ASTM F 2066-08, Standard specification for wrought titanium 15molybdenum alloy for surgical implant applications (ASTM, Philadelphia, 2008).
[17]J. R. S. Martins Júnior, R. A. Nogueira, R. O. d. Araújo, T. A. G. Donato, V. E. Arana-Chavez, A. P. R. A. Claro, J. C. S. Moraes, M. A. R. Buzalaf, and C. R. Grandini, Mater. Res. **14**, 107–112 (2011).
[18]P. J. Bania, in *Titanium Alloys in the 1990's*, edited by D. Eylon, R. R. Boyer, and D. A. Koss (The Mineral, Metals & Materials Society, Warrendale, 1993).
[19]B. D. Cullity and S. R. Stock, *Elements of X-Ray Diffraction*, 3rd ed. (Prentice-Hall, New York, 2001).
[20]D. Lide, *CRC Handbook of Chemistry and Physics: A Ready-Reference Book of Chemical and Physical Data* (CRC, 2004).
[21]H. M. Rietveld, J. Appl. Crystallogr. **2**, 65–71 (1969).
[22]R. J. Hill and C. J. Howard, J. Appl. Crystallogr. **20**, 467–474 (1987).
[23]A. C. Larson and R. B. V. Dreele, General Structure Analysis System (GSAS), Los Alamos National Laboratory Report LAUR 86-748 (2004).
[24]See www.portaldapesquisa.com.br/databases/sites for ICSD, Vol. 2010 (2010).
[25]S. Banumathy, R. K. Mandal, and A. K. Singh, J. Appl. Phys. **106**(9), 093518–093516 (2009).
[26]G. K. Williamson and W. H. Hall, Acta Metall. **1**(1), 22–31 (1953).